# NUMERICAL METHOD TO CALCULATE THE INDUCED DRAG OR OPTIMUM LOADING FOR ARBITRARY NON-PLANAR AIRCRAFT

James A. Blackwell, Jr.
Lockheed-Georgia Company

## SUMMARY

A simple unified numerical method applicable to non-planar subsonic aircraft has been developed for calculating either the induced drag for an arbitrary loading or the optimum aircraft loading which results in minimum induced drag. The method utilizes a vortex lattice representation of the aircraft lifting surfaces coupled with the classic equations and theorems for computing and minimizing induced drag. Correlation of results from the numerical method with non-planar solutions obtained from other more complex theories indicates very good agreement. Comparison of the induced-drag computations using the numerical method with experimental data for planar and non-planar configurations was also very good.

4

## INTRODUCTION

Over the past few years, increased attention has been focused on improving aircraft performance. One method to improve performance is to lower the aircraft induced drag. This can be accomplished by more efficient design of conventional configurations or by developing new and unique designs whose intent is to minimize induced drag. Typical of new configurations that have been developed for this purpose are the Lockheed boxplane and the Whitcomb winglet configuration.

The aircraft lifting surfaces for conventional aircraft as well as for new configurations are generally non-planar in design. To achieve a minimum induced drag, these non-planar surfaces must be designed to support the required optimum loads as specified by classical theory (refs. 1 and 2). Unfortunately, the use of classical theory to determine the design loads is quite cumbersome since rather complex conformal transformations must be utilized. Thus, a simple inexpensive method is required to determine what the "design to" loading of a non-planar configuration should be to minimize the aircraft induced drag. Furthermore, for conditions where the aircraft is not operating at design conditions, an analysis method is required to quickly assess the magnitude of the aircraft off-design induced drag. Also, methods of this type are of particular importance in making configurational trade-offs.

The objective of this paper is to present a simple unified numerical method applicable to subsonic non-planar aircraft for the rapid calculation of:

1. the induced drag for an arbitrary aircraft loading or

2. the optimum aircraft loading which results in minimum induced drag.

The paper will include a discussion of the fundamental theoretical concepts on which the method is based, followed by the theoretical formulation of the numerical calculation procedure. Computations will be made using the method and will be compared to existing theoretical solutions and to experimental data. This will be followed by an illustration of the utility of the method for making configurational trade-offs by comparing the loading and induced drag results for various types of wing additions such as winglets or wing-tip extensions.

## SYMBOLS

| | |
|---|---|
| $A_{ij}$ | geometric influence function |
| AR | aspect ratio, $b^2/S$ |
| b | reference span |
| c | local chord of lifting surface |
| $c_{AV}$ | average chord (S/b) |
| $c_n$ | section load coefficient normal to load perimeter |
| $C_L$ | lift coefficient |
| $C_{D_i}$ | induced drag coefficient |
| $C_{WB}$ | bending-moment coefficient |
| $D_i$ | induced drag ($D_i = C_{D_i}\ qS$) |
| e | efficiency factor |
| F | resultant force of lifting surface |
| h | length of wing addition |
| $\bar{k}$ | unit normal vector parallel to Z axis |
| $\ell$ | length of load perimeter |
| L | lift force ($L = C_L\ qS$) |
| M | Mach number |

| | |
|---|---|
| m | number of lifting elements on load perimeter |
| $\bar{n}$ | unit vector normal to load perimeter |
| N | section load normal to load perimeter ($N = q\ c_n\ c$) |
| q | free-stream dynamic pressure |
| s' | semi-width of vortex pair |
| s | nondimensional semi-width of vortex pair ($s = 2s'/b$) |
| S | reference area |
| S.F. | side force |
| u,v,w | induced velocities |
| V | resultant induced velocity |
| $V_n$ | velocity normal to load perimeter |
| $V_\infty$ | free-stream velocity |
| Y', Z' | lifting element coordinate system |
| X, Y, Z | aircraft coordinate system |
| $y_{cp}$ | aircraft spanwise center of pressure |
| $\Gamma$ | circulation (eq. (10)) |
| $\theta$ | rotation angle in the Y-Z plane |

Superscript:

| | |
|---|---|
| - | indicates vector quantity |

Subscripts:

| | |
|---|---|
| i | number designating a vortex pair that model a particular lifting element |
| j | number designating a control point on a particular lifting element |
| w | wing |
| wl | winglet |

## BASIC THEORETICAL CONCEPTS

Fundamental to the development of the present model is the representation of the aircraft non-planar lifting surfaces by a system of rectangular horseshoe vortices (ref. 3). The induced drag for a given loading or the optimum loading for minimum induced drag can be calculated for any arbitrary non-planar aircraft at subsonic speeds utilizing this vortex representation and the following basic law and theorems: Munk's Theorems I to III, Biot-Savart Law, and the Kutta-Joukowski Theorem.

Munk's first theorem (ref. 1) can be stated as follows:

> *The total induced drag of any multiplane system is unaltered if any of the lifting elements are moved in the direction of motion provided that the attitude of the elements is adjusted to maintain the same distribution of lif' among them.*

This theorem is commonly referred to as Munk's stagger theorem. An illustration of this theorem is shown in figure 1. Several practical applications can be deduced from this theorem. First, the chordwise distribution of pressure does not affect the theoretical induced drag of the aircraft if constant section lift is maintained. Second, wing sweep does not effect the theoretical induced drag as long as the spanwise distribution of lift is constant. A third application is that the load from a system of multi-surfaces (i.e. wing and horizontal tail) with the same projection in the Y-Z plane can be made equivalent to a single surface for the purpose of calculating induced drag.

In the following theoretical development, use will be made of Munk's first theorem to lump the chordwise distribution of vorticity into a single chordwise load and to translate all loads into the O,Y,Z plane (fig. 1).

Munk's second theorem (ref. 1) is illustrated in figure 2 and can be stated as:

> *In calculating the total induced drag of a lifting system, once all the forces have been concentrated into the plane O,Y,Z, we may, instead of using the actual values of the velocity normal to the lifting elements* $[V_n(x,y,z)]$ *at the original points of application of the forces, use one-half the limiting value of the normal velocity* $[V_n(\infty,y,z)]$ *for the corresponding values at points* $P(0,y,z)$.

This theorem allows the computations to be done in the Trefftz plane (downstream infinity) rather than in the real plane. In the subsequent theoretical derivation, this fact will be utilized to make all the computations in the Trefftz plane, thereby greatly simplifying the calculations.

The third theorem given by Munk (ref. 1) is presented as follows:

*When all the elements of a lifting system have been translated longitudinally to a single plane, the induced drag will be a minimum when the component of the induced velocity normal to the lifting element at each point is proportional to the cosine of the angle of inclination of the lifting element at that point.*

This theorem is illustrated in figure 3 and can be summarized in equation form as:

$$V_n = w_o \cos\theta \tag{1}$$

For a horizontal lifting element it can be seen from equation (1) that the normal velocity (downwash) across the span is equal to a constant (fig. 3). For a vertical plane ($\theta = 90°$), the normal velocity (sidewash) must be equal to zero for minimum induced drag. The physical interpretation of this theorem will be further illustrated in a subsequent section.

Equation (1) will be utilized in the following theoretical development as the boundary condition necessary to achieve a minimum induced drag and hence an optimum aircraft loading.

The basic equation for calculating the aircraft-induced drag can be derived by applying the Kutta-Joukowski theorem in the drag direction. By virtue of Munk's theorems, the calculations can be accomplished in the Trefftz plane rather than the real plane. Thus, the equation for induced drag expressed in terms of the Trefftz plane variables and using vector notation is:

$$D_i = \frac{1}{2V_\infty} \oint \bar{V} \cdot N\bar{n} \, d\ell \tag{2}$$

Equation (2) along with the induced velocities in the Trefftz plane derived from the vortex model of the lifting surfaces will comprise the basis for the induced drag computation.

## PHYSICAL INTERPRETATION OF THEORETICAL CONCEPTS

To provide a better physical understanding of the computation of induced drag and the calculation of the optimum loading for minimum induced drag, the theoretical concepts discussed in the previous section will be illustrated using a wing-winglet configuration. In figure 4, the sources of induced drag for a wing-winglet combination are shown. These are:

- Drag due to the induced flow by the wings on the wing
- Drag due to the induced flow by the wings on the winglet

- Drag due to the induced flow by the winglets on the winglet
- Drag due to the induced flow by the winglets on the wing

For simplicity, the effects of symmetry are included in the sources of induced drag shown and are not delineated separately.

In figure 4(a), the effect of the wing induced flow is shown. The wing under positive load produces a downwash on itself which results in the wing force vector, $\bar{F}$, tilting rearward by an angle $\alpha_i$. The wing force vector, $\bar{F}$, is perpendicular to the resultant, V, (Kutta-Joukowski theorem). The rearward rotation of the force vector results in a wing-induced drag. A sidewash is also produced by the wing at the winglet location. As can be seen in figure 4(b), the sidewash from the wing combined with the free-stream velocity produces a tilt forward of the winglet force resulting in a thrust component.

In figure 4(c), the induced drag resulting from the sidewash of the winglet on itself is presented. This results in a rearward tilting of the winglet force vector and an attendant induced drag. It should be noted that the direction of the winglet force vector is consistent with a positive (upload) on the wing. The winglet also induces an upwash on the wing. In figure 4(d), it can be seen that this upwash rotates the wing force vector forward producing a thrust force.

The results from figure 4 are summarized in figure 5, where all the induced velocities are combined. For minimum induced drag, equation (1) indicates that the velocity normal to the winglet must be equal to zero ($\theta = 90°$). This can be seen to occur when the sidewash produced on the winglet by the wing exactly cancels the sidewash produced by the winglet on itself. In other words, the induced angle of attack ($\alpha_i$) of the winglet is zero. The induced drag of the wing is also minimized by the presence of a winglet since the winglet causes a reduction in the net downwash at the wing; and, hence, the induced angle of attack is reduced.

## DERIVATION OF NUMERICAL METHODS

### Vortex Model

By virtue of Munk's theorems, the calculations for induced drag and the optimum loading can be accomplished in the Trefftz plane. This fact considerably simplifies the calculation problem since the method will not be a function of the longitudinal coordinate. The projection of the aircraft non-planar lifting surfaces in the Trefftz plane will be referred to as the load perimeter.

In the real plane, the aircraft lifting surfaces will be represented by a system of horseshoe vortices. The equations describing the induced velocities in the Trefftz plane at a control point $P(\infty,y_i,z_i)$ (fig. 6) due to a horseshoe

vortex located in the real plane at a point $P(x_j, y_j, z_j)$ are given below as derived from the Biot-Savart Law (ref. 3):

$$\frac{u_i}{V_\infty} = 0 \tag{3}$$

$$\frac{v_i}{V_\infty} = -\frac{1}{2\pi}\frac{\Gamma_j}{V_\infty}\left(\frac{z'}{R_1} - \frac{z'}{R_2}\right) \tag{4}$$

$$\frac{w_i}{V_\infty} = \frac{1}{2\pi}\frac{\Gamma_j}{V_\infty}\left(\frac{(y'-s')}{R_1} - \frac{(y'+s')}{R_2}\right) \tag{5}$$

where

$$R_1 = (z')^2 + (y'-s')^2 \tag{6}$$

$$R_2 = (z')^2 + (y'+s')^2 \tag{7}$$

$$y' = (y_i - y_j)\cos\theta_j + (z_i - z_j)\sin\theta_j \tag{8}$$

$$z' = -(y_i - y_j)\sin\theta_j + (z_i - z_j)\cos\theta_j \tag{9}$$

and the circulation by virtue of the Kutta-Joukowski theorem is given as

$$\frac{\Gamma_j}{V_\infty} = \frac{(c_n\, c)_j}{2} \tag{10}$$

Inspection of equations (3) to (5) indicates that there is no contribution from the horseshoe bound leg in the Trefftz plane and the induced velocities are not dependent on x. The resulting model then reduces to describing the load perimeter in the Trefftz plane (fig. 6) by lifting elements that are represented by a trailing vortex pair having a circulation of equal magnitude but of opposite rotation. For each lifting element there is an associated control point located midway between the pair of vortices.

## Induced Drag Calculation

The basic equation for calculating the induced drag for an arbitrary nonplanar lifting system was given in equation (2) as:

$$D_i = \frac{1}{2V_\infty}\oint \bar{V}\cdot N\bar{n}\, d\ell$$

The integral is a circuit integral taken around the perimeter of the projection of the lifting system in the Trefftz plane. The vector $\bar{V}$ is the resultant induced velocity vector in the Trefftz plane from all vortices on the load perimeter. The vector $\bar{n}$ is a unit vector, normal to the load perimeter.

Reducing equation (2) to coefficient form, nondimensionalizing the lifting element length ($\ell$) by the reference semispan, and using the relationship for the average chord, the following result is obtained

$$C_{D_i} = \frac{1}{4} \oint \frac{\bar{V}}{V_\infty} \cdot \left(\frac{c_n\, c}{c_{AV}}\right) \bar{n}\, d\left(\frac{2\ell}{b}\right) \tag{11}$$

Writing the above in the form of a sum and assuming symmetry about the X-Z plane

$$C_{D_i} = \frac{1}{2} \sum_{i=1}^{m} \frac{(c_n\, c)_i}{c_{AV}} \frac{[V \cos(\bar{V},\bar{n})]_i}{V_\infty} \Delta(2\ell/b)_i \tag{12}$$

where m equals the number of elements that comprise the load perimeter. Writing equation (12) in terms of the nondimensional lifting element semi-width(s) and noting that

$$V_n = V\cos(\bar{V},\bar{n}) \tag{13}$$

the expression for induced drag can be written as

$$C_{D_i} = \sum_{i=1}^{m} \frac{V_{n_i}}{V_\infty} \frac{(c_n\, c)_i}{c_{AV}}\, s_i \tag{14}$$

The velocities normal to the lifting elements ($V_n$) can be determined by utilizing the expressions for the induced velocities in equations (4) and (5).

From the geometry of figure 6, the normal velocity at $P_i$ due to a vortex pair at $P_j$ can be expressed in terms of the induced velocities as:

$$\frac{V_{n_i}}{V_\infty} = \frac{w_i}{V_\infty} \cos(\theta_i - \theta_j) - \frac{v_i}{V_\infty} \sin(\theta_i - \theta_j) \tag{15}$$

Combining equations (4), (5), (10), and (15) yields the expression for the total normal velocity at the control point $P_i$ due to vortices at all points $P_j$:

$$\frac{V_{n_i}}{V_\infty} = \sum_{j=1}^{m} \frac{(c_n\, c)_j}{c_{AV}} \left\{ \frac{c_{AV}}{4\pi} \left(\frac{(y'-s')}{R_1} - \frac{(y'+s')}{R_2}\right) \cos(\theta_i - \theta_j) \right.$$

$$\left. + \frac{c_{AV}}{4\pi} \left(\frac{z'}{R_1} - \frac{z'}{R_2}\right) \sin(\theta_i - \theta_j) \right\} \tag{16}$$

The portion contained in curvy brackets is only a function of the projected aircraft geometry in the Trefftz plane and will be denoted by $A_{ij}$. Thus, in terms of the geometric influence function $A_{ij}$,

$$\frac{V_{n_i}}{V_\infty} = \sum_{j=1}^{m} \frac{(c_n\, c)_j}{c_{AV}} A_{ij} \tag{17}$$

Substitution of equation (17) into equation (14) yields the final expression for the induced drag:

$$C_{D_i} = \sum_{i=1}^{m} \sum_{j=1}^{m} \left(\frac{(c_n\, c)_j}{c_{AV}}\right) \left(\frac{(c_n\, c)_i}{c_{AV}}\right) (s_i)(A_{ij}) \tag{18}$$

The independent parameters in equation (18) are the loadings normal to the load perimeter, the lifting element semi-widths, and the geometric influence function. The loading normal to the load perimeter will be considered input to the present method. The normal loading can be determined from any available non-planar lifting surface calculation procedure such as in reference 3 or from experimental data. The lifting element semi-width is also considered as input. The geometric influence function ($A_{ij}$), as has been previously mentioned, is a function of the input aircraft geometry.

For an arbitrary applied load, the lift can be determined from the following expression

$$L = \oint N\bar{n} \cdot \bar{k}\, d\ell \tag{19}$$

Expressing equation (19) in coefficient form and writing as a sum

$$C_L = 2 \sum_{j=1}^{m} \left(\frac{(c_n\, c)_j}{c_{AV}}\right) (s_j) \cos(\bar{n}_j, \bar{k}) \tag{20}$$

Since

$$\cos(\bar{n}_j, \bar{k}) = \cos \theta_j \tag{21}$$

the final expression for the lift coefficient is given by

$$C_L = 2 \sum_{j=1}^{m} \left(\frac{(c_n\, c)_j}{c_{AV}}\right) (s_j) \cos \theta_j \tag{22}$$

The bending-moment coefficient at the X-axis can be expressed as

$$C_{WB} = \frac{1}{2} \sum_{j=1}^{m} \left(\frac{(c_n\, c)_j}{c_{AV}}\right) s_j \left(\frac{y_j}{b/2} \cos\theta_j + \frac{z_j}{b/2} \sin\theta_j\right) \tag{23}$$

The spanwise center-of-pressure location can be determined from the following equation:

$$\frac{y_{cp}}{b/2} = \frac{4C_{WB}}{C_L} \tag{24}$$

The aircraft efficiency factor can be calculated from the following standard equation:

$$e = \frac{C_L{}^2}{\pi\ AR\ C_{D_i}} \tag{25}$$

Optimum Load Calculation

The expression for the total velocity normal to a lifting element was given in equation (17) as:

$$\frac{V_{n_i}}{V_\infty} = \sum_{j=1}^{m} \frac{(c_n\ c)_j}{c_{AV}}\ A_{ij}$$

According to Munk's theorem III, the loading for minimum induced drag is obtained when the distribution of normal velocity satisfies equation (1):

$$\frac{V_{n_i}}{V_\infty} = \frac{w_o}{V_\infty} \cos\theta_i$$

where $w_o$ is a constant. Using equation (1) as a boundary condition and combining it with equation (17), there results:

$$\frac{w_o}{V_\infty} \cos\theta_i = \sum_{j=1}^{m} \frac{(c_n\ c)_j}{c_{AV}}\ A_{ij} \tag{26}$$

where the loading in equation (26) is the optimum loading. Using square brackets to indicate matrix notation, equation (26) can be written as:

$$\left[\cos\theta_i\right] = \frac{1}{w_o/V_\infty}\left[A_{ij}\right]\left[\frac{(c_n\ c)_j}{c_{AV}}\right] \tag{27}$$

Solving for the optimum loading

$$\left[\frac{(c_n\ c)_j}{c_{AV}}\right] = \frac{w_o}{V_\infty}\left[A_{ij}\right]^{-1}\left[\cos\theta_i\right] \tag{28}$$

The value of the arbitrary constant, $w_o$, can be determined from equation (22) by specifying the aircraft lift coefficient.

In summary, to determine the loading for minimum induced drag, only the lift coefficient and aircraft geometry are required for input. Once the

loading has been determined, the minimum induced drag, the spanwise center-of-pressure location, and efficiency can be determined in the manner previously presented (eqs. (18), (24), and (25)).

## CORRELATION OF METHOD

The theory described in the previous section for calculating the aircraft induced drag for a given loading or the loading for a minimum induced drag has been coded for use on Lockheed computers. In this section, computations using the present method will be compared to other theoretical solutions and to experimental results.

### Induced-Drag Correlations

Numerical solutions for the aircraft efficiency for a monoplane of aspect ratio eight are shown in figure 7 for various values of lifting element widths. For this example, the widths of the elements over the load perimeter were held constant. A more efficient result could have been obtained if, for instance, a cosine spacing of the elements had been used. The input loading on the monoplane was specified to be elliptical. The exact solution for the efficiency factor (ref. 1) on an elliptically loaded monoplane is, of course, 1.0. As can be seen, the numerical solution approaches the exact value as the width of the elements become smaller. For a lifting element width equal to .01 (b/2), the error was approximately 0.5% in efficiency.

A similar calculation was made for an aspect ratio eight biplane with wings of equal span and a height-to-span ratio of 0.5. The biplane was loaded optimally utilizing the loadings derived in reference 1, based on transformation theory. The numerical calculation for efficiency factor was 1.6307 (using constant elements of 0.0125(b/2) in width) compared to the value of 1.6260 given in reference 1. The resulting difference was approximately 0.3%.

In figure 8, induced-drag results calculated using the present method are compared to the experimental results for an advanced Lockheed transport designed to cruise at 0.95 Mach number and at a lift coefficient of 0.47. The spanwise loading for the aircraft was obtained from an available lifting surface program similar to that in reference 3. As can be seen, the agreement between theory and experiment is very good over a range near the design lift coefficient.

A further correlation example is presented in figure 9 where numerical results are compared with experimental data for a non-planar Lockheed boxplane configuration. Again, the loading was obtained from lifting-surface theory. As indicated, good agreement is obtained.

### Optimum Load Correlations

In figure 10 the optimum loading is presented for an aspect ratio eight monoplane as calculated from equation (28) using constant elements of .01(b/2)

in width. Also shown is the classic optimum result for a monoplane – an elliptical loading. The correlation can be seen to be very good. The error in induced drag of the computed result was approximately 0.5%, which is consistent with the results in figure 7.

In reference 2, an optimum loading for a wing with a winglet is presented as derived from transformation theory. This solution is compared to the result calculated using the present method in figure 11. Good agreement between the two methods is obtained.

## ILLUSTRATIVE USE OF METHOD

Taken together, the present numerical method provides a unique tool for understanding the sources of induced drag and making configuration trade-offs to achieve an overall aerodynamic as well as structurally optimum aircraft. An illustration of using the method to provide additional understanding into the basic sources and mechanisms of induced drag is presented in figure 12, where the magnitude of the induced-drag components for a wing-winglet configuration (fig. 4) with optimum load is presented. From the figure, it can be seen that the induced-drag contribution from the wing on the winglet and the winglet on the winglet are of the same magnitude and cancel each other. This is, of course, the result previously illustrated in figure 5.

As a result of design or structural constraints, the aircraft may not be able to achieve the optimum loading for minimum induced drag. The penalties that incur from the use of non-optimum loadings can be quickly assessed using the present method. This is illustrated in figure 13, where the winglet loading for a wing-winglet configuration is varied. As can be seen the induced drag is sensitive to certain types of changes (non-optimum 1) where it is not to others (non-optimum 2).

The present method can also be used to quickly make configuration trade-offs. This is illustrated in figures 14 and 15. In figure 14 the parametric effect of wing additions on induced drag and on the wing spanwise center-of-pressure location as calculated from the present method are presented. If, for instance, it was desired to find a configuration which would give the maximum induced drag reduction for a minimum outboard shift in wing center of pressure, this can quickly be determined by replotting the parametric data of figure 14 in the form of figure 15 and the result determined.

## CONCLUDING REMARKS

A unified numerical method applicable to non-planar subsonic aircraft has been developed for the purpose of calculating the induced drag for an arbitrary loading or the optimum aircraft loading that gives minimum induced drag.

Use of the numerical method has indicated that:

(1) the method is simple and easy to use

(2) induced drag and optimum loading results from the numerical method correlate very well with non-planar solutions obtained from more complex theories

(3) numerical induced-drag predictions are in good agreement with experimental data for planar and non-planar configurations

(4) the numerical method provides both analysis and design capability which allows the designer to make rapid configuration assessments and trade-offs for the purpose of achieving an overall aerodynamic as well as structurally optimum aircraft.

## REFERENCES


1. Durand, W. F. (ed.): Aerodynamic Theory. Dover Publications, Inc., New York, 1963, Volume II, Division E.

2. Lundry, J. L.: A Numerical Solution for the Minimum Induced Drag and the Corresponding Loading of Nonplanar Wings. NASA CR-1218, November 1968.

3. Blackwell, James A. Jr.: A Finite-Step Method for Calculation of Theoretical Load Distributions for Arbitrary Lifting-Surface Arrangements at Subsonic Speeds. NAS TN D-5335, July 1969.

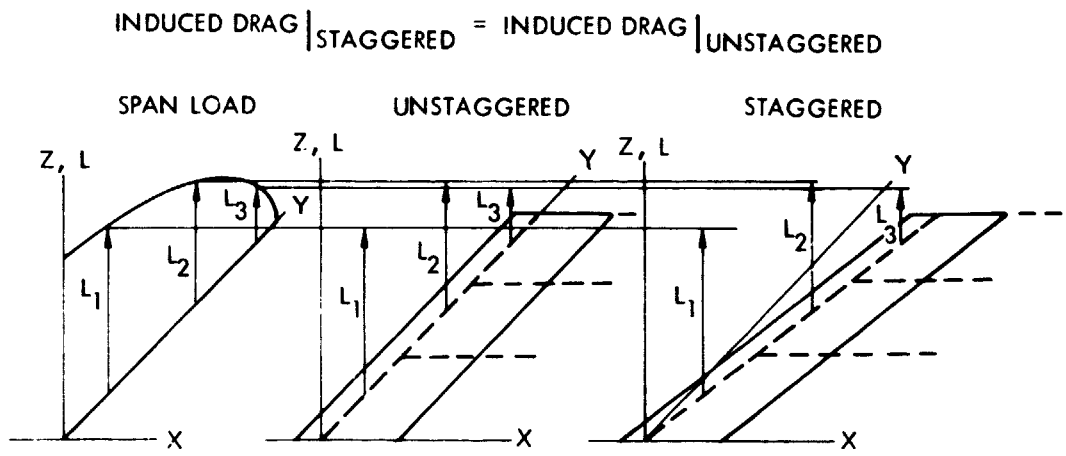


Figure 1.- Illustration of Munk's theorem I.

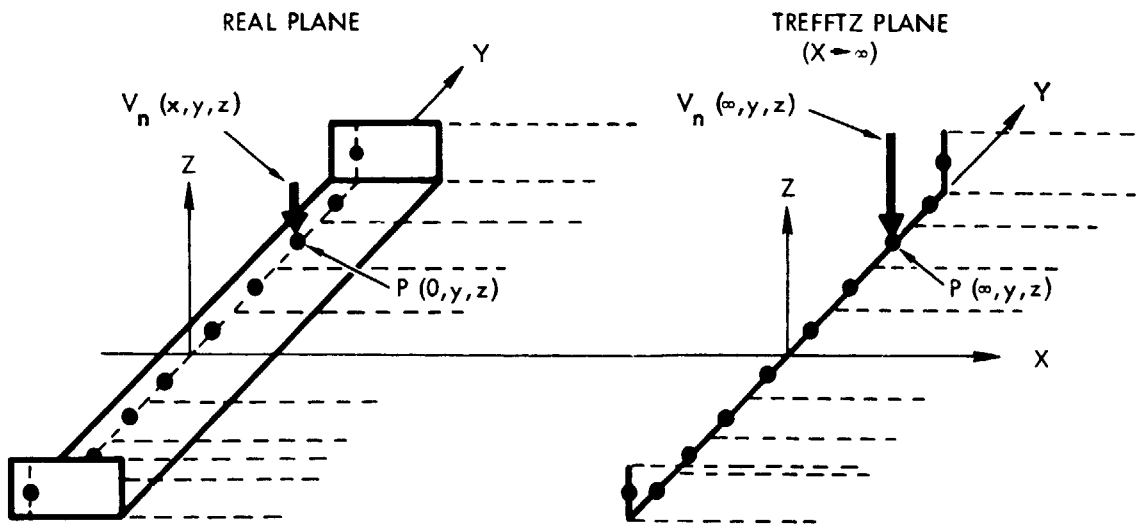


Figure 2.- Illustration of Munk's theorem II.

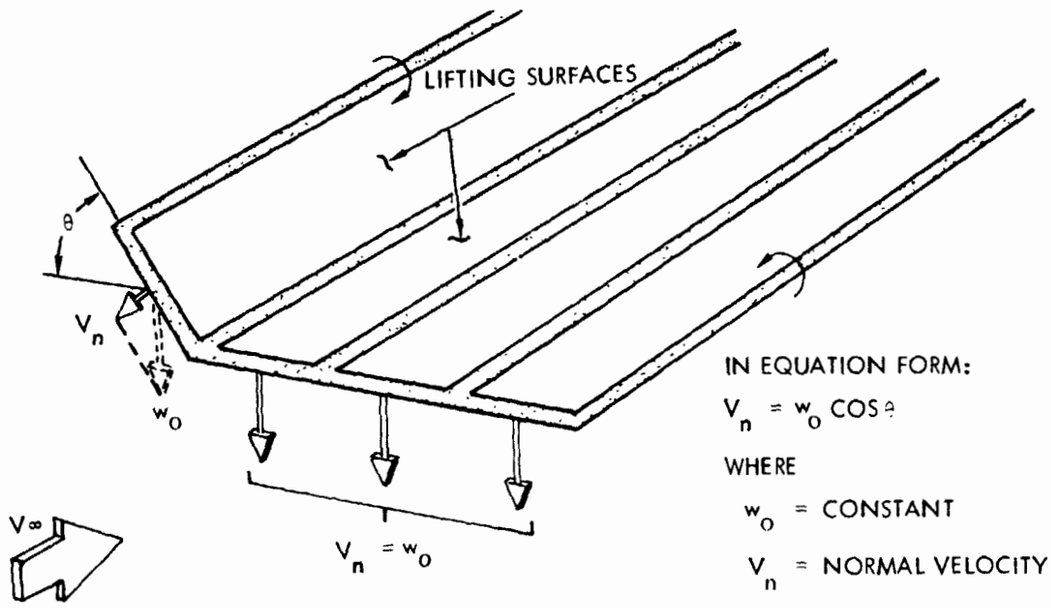


Figure 3.- Illustration of Munk's theorem III.

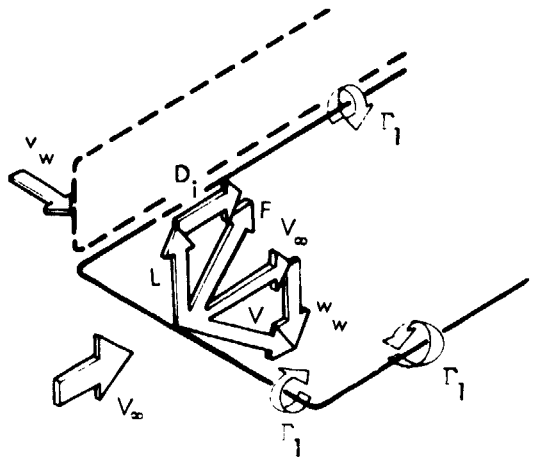


(a) Drag due to wing on wing $D_{i_{w,w}}$.

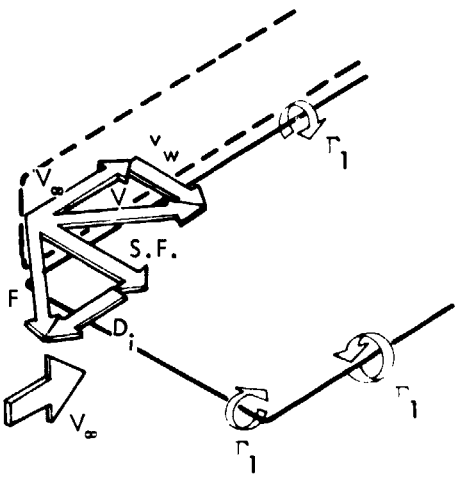


(b) Drag due to wing on winglet $D_{i_{w,w\ell}}$.

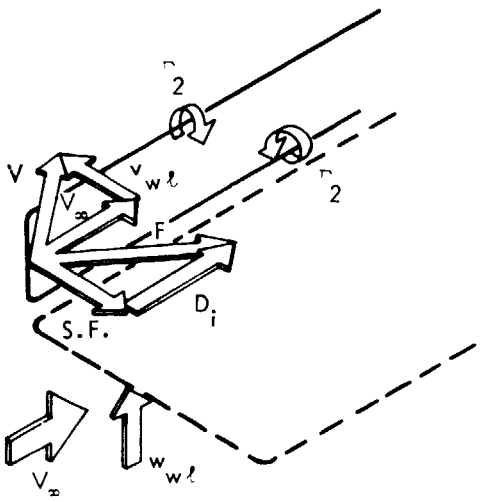


(c) Drag due to winglet on winglet $D_{i_{w\ell,w\ell}}$.

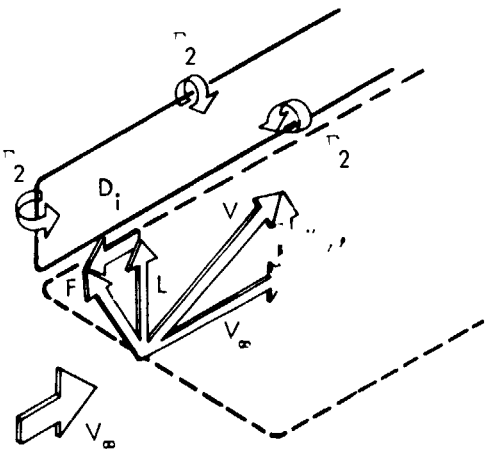


(d) Drag due to winglet on wing $D_{i_{w\ell,w}}$.

Figure 4.- Sources of induced drag for a wing/winglet configuration.

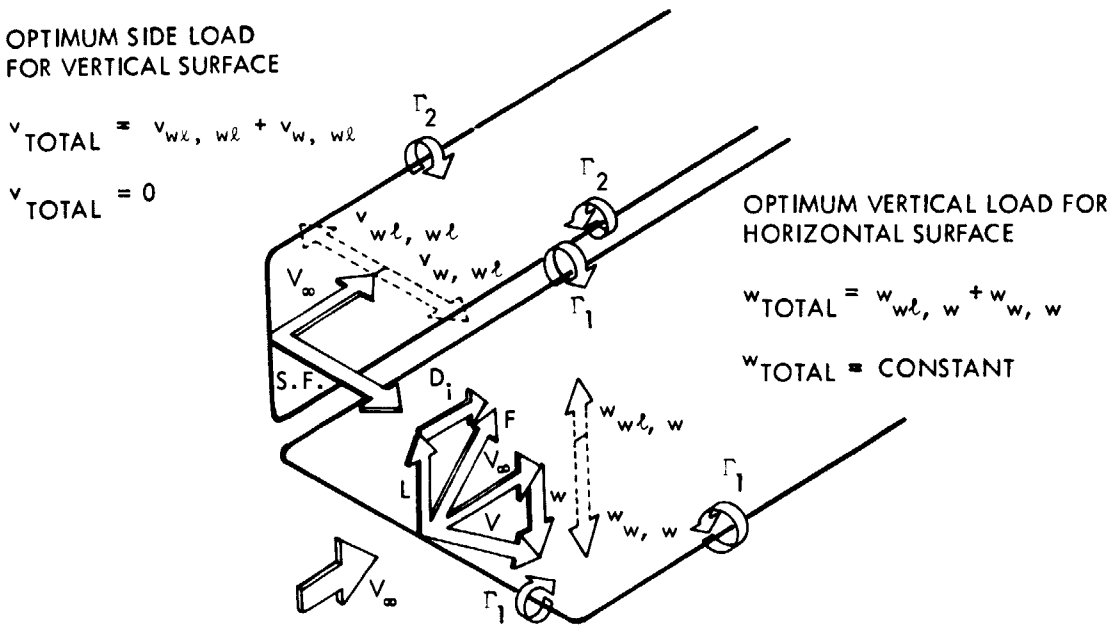


Figure 5.- Combined sources of induced drag for a wing/winglet configuration.

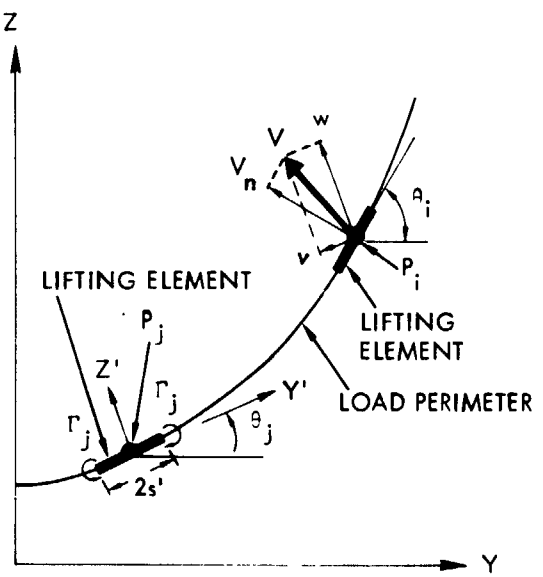


Figure 6.- Induced velocities in the Trefftz plane.

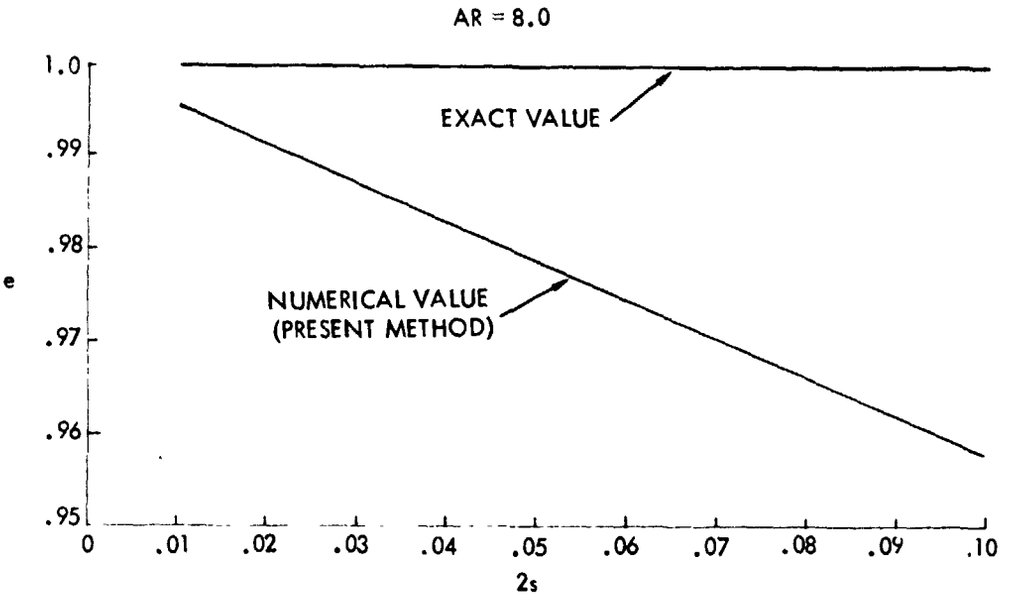


Figure 7.- Variation of efficiency for optimally loaded monoplane.

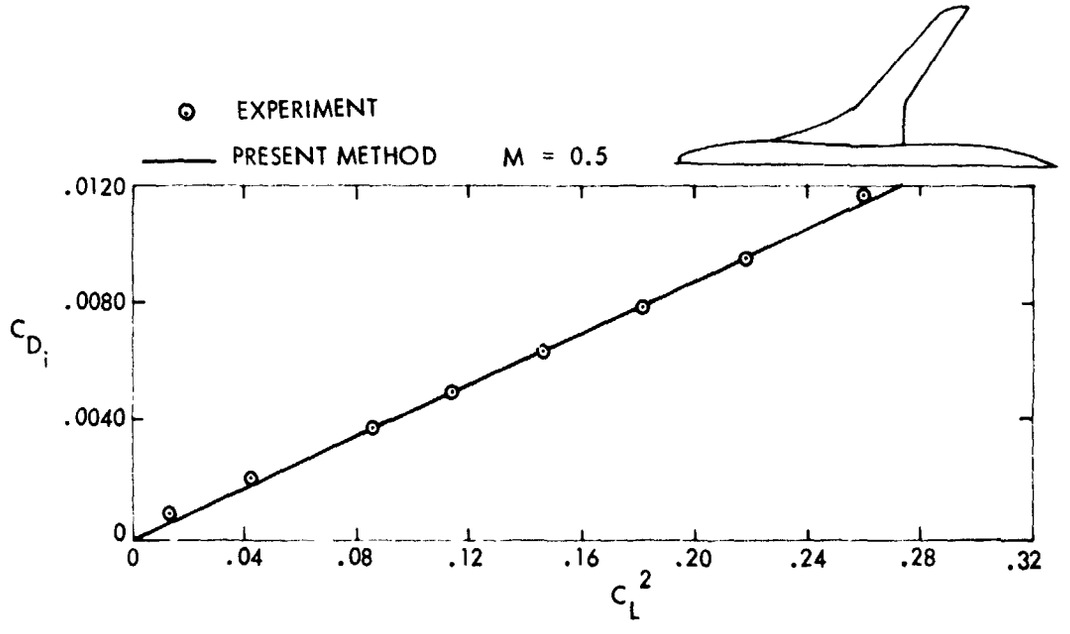


Figure 8.- Induced drag for Lockheed ATT-95 aircraft.

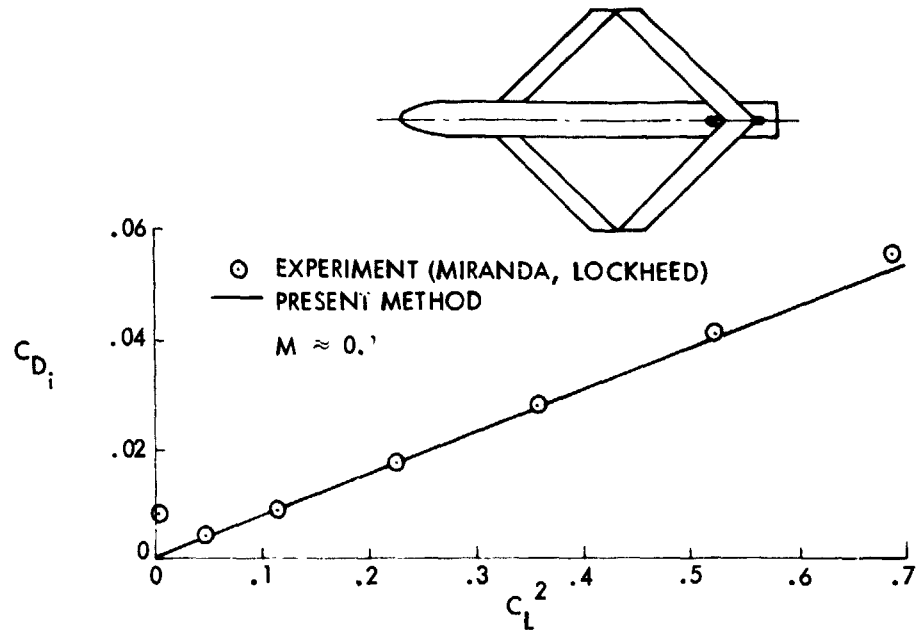


Figure 9.- Induced drag for a Lockheed boxplane.

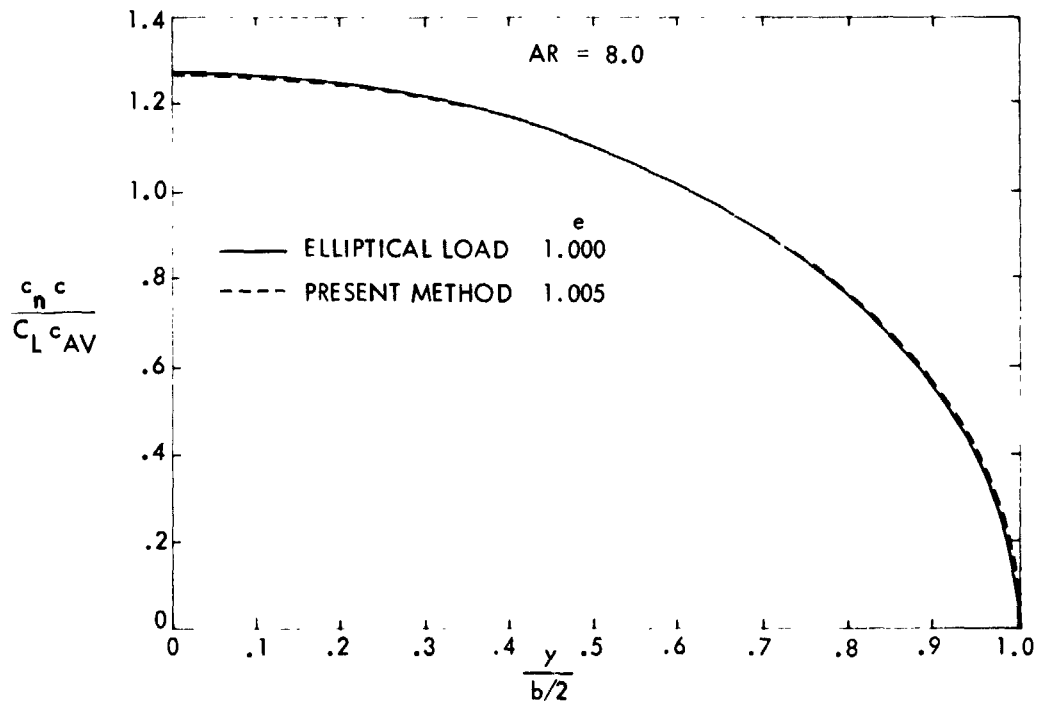


Figure 10.- Comparison of numerical and exact optimum span loadings for a monoplane.

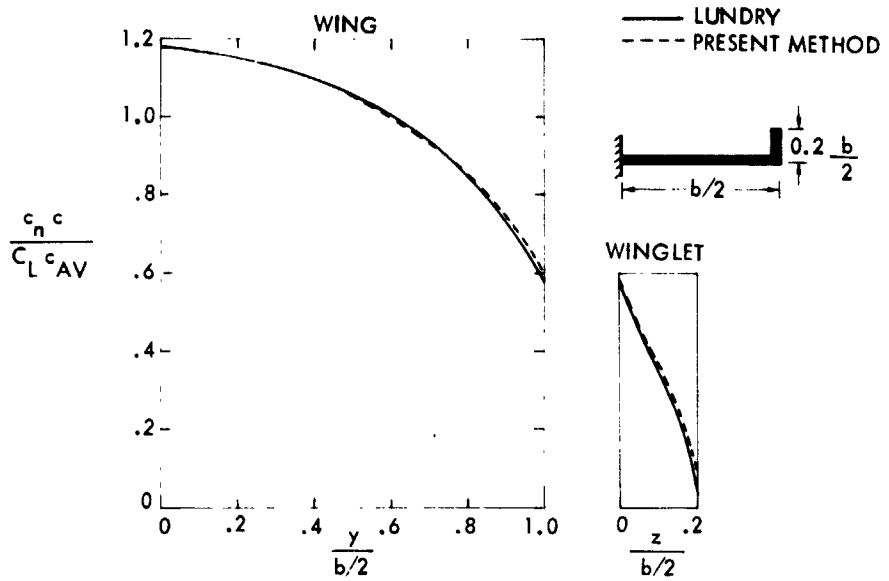


Figure 11.- Comparison of theoretical optimum loadings for a wing/winglet configuration.

$C_L = 1.0$
AR = 10.0

| WING - WINGLET | WING ALONE |
|---|---|
| (1) $C_{D_{i_{w,w}}} = +.0369$ | $C_{D_i} = +.0318$ |
| (2) $C_{D_{i_{w,wl}}} = -.0110$ | |
| (3) $C_{D_{i_{wl,wl}}} = +.0110$ | |
| (4) $C_{D_{i_{wl,w}}} = -.0109$ | |
| $\Sigma C_{D_i} = +.0260$ | |

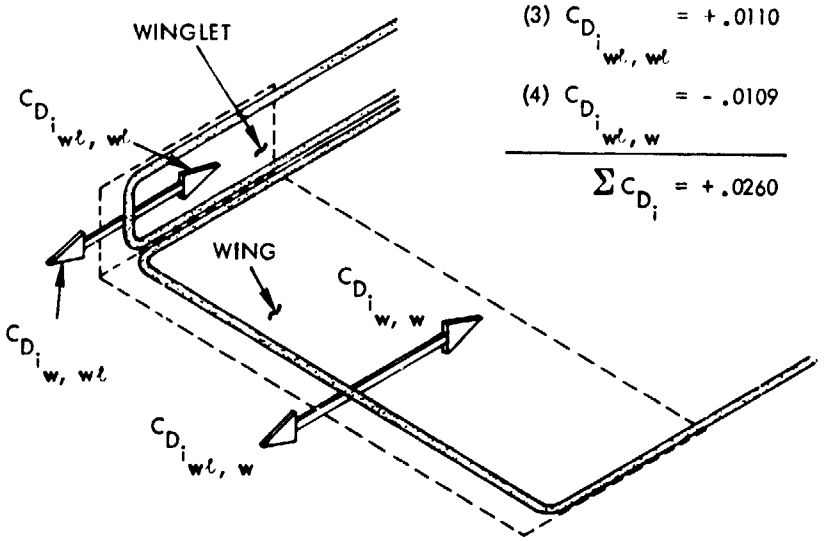


Figure 12.- Illustration of induced drag calculations for a wing/winglet configuration.

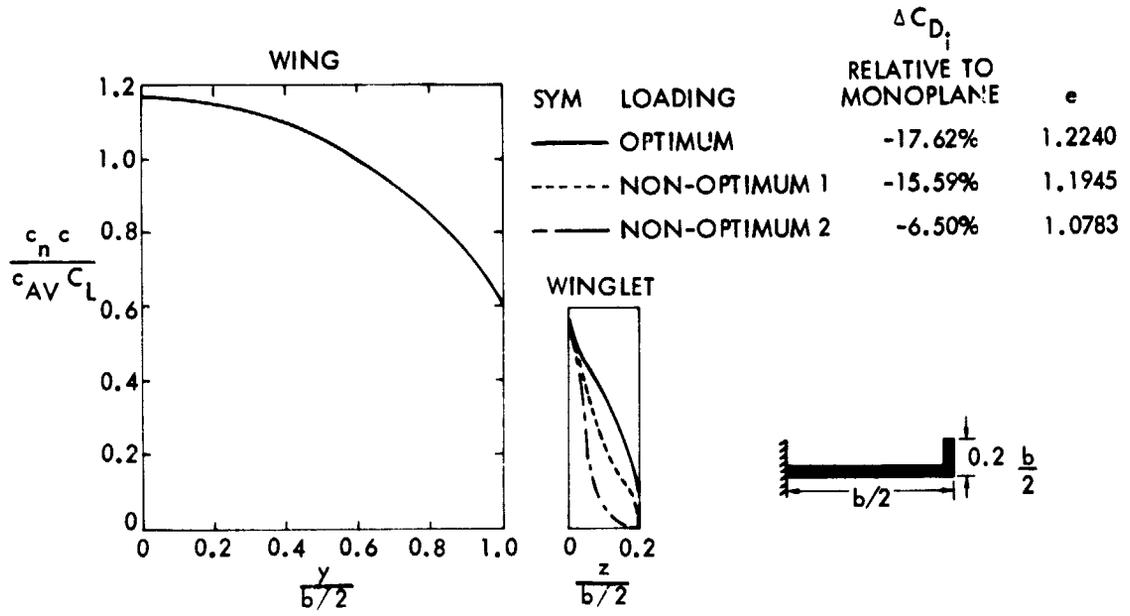


Figure 13.- Effect of changes in winglet loading on the induced drag of a wing/winglet configuration.

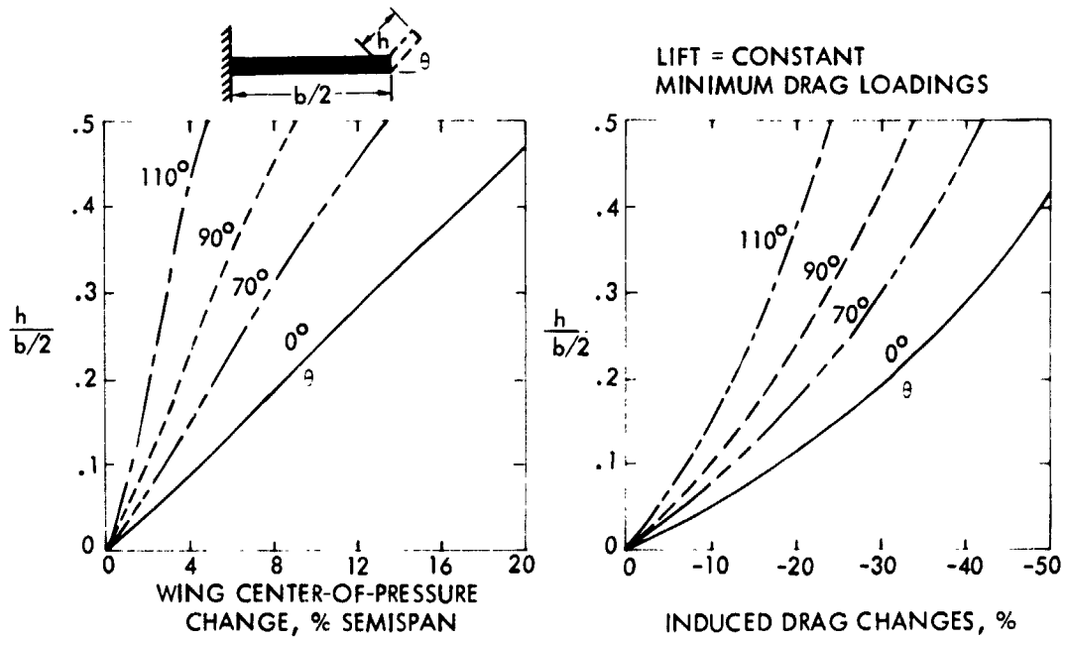


Figure 14.- Basic theoretical effects due to wing additions.

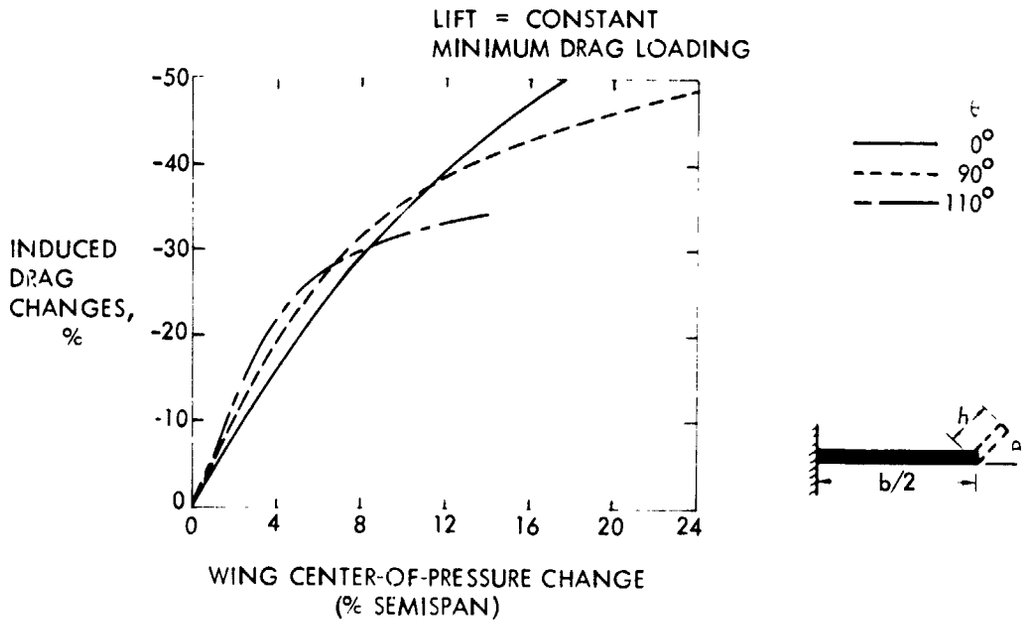


Figure 15.- Theoretical effect of wing additions for various dihedral angles.